We are IntechOpen, the world's leading publisher of Open Access books Built by scientists, for scientists

4,800
Open access books available

122,000
International authors and editors

135M
Downloads

Our authors are among the

154
Countries delivered to

TOP 1%
most cited scientists

12.2%
Contributors from top 500 universities

CLARIVATE ANALYTICS BOOK CITATION INDEX INDEXED

WEB OF SCIENCE™

Selection of our books indexed in the Book Citation Index in Web of Science™ Core Collection (BKCI)

Interested in publishing with us?
Contact book.department@intechopen.com

Numbers displayed above are based on latest data collected.
For more information visit www.intechopen.com

2

Photonic Quantum Ring Laser of Whispering Cave Mode

O'Dae Kwon, M. H. Sheen and Y. C. Kim
Pohang University of Science & Technology
S. Korea

1. Introduction

In early 1990s, an AT&T Bell Laboratory group developed a microdisk laser of thumb-tack type based upon Lord Rayleigh's 'concave' whispering gallery mode (WGM) for the optoelectronic large-scale integration circuits (McCall et al., 1992). The above lasers were however two dimensional (2D) WGM which is troubled with the well-known WGM light spread problem. For the remedy of this problem, asymmetric WGM lasers of stadium type (Nockel & Stone, 1997) were then introduced to control the spreading light beam. Quite recently, a novel micro-cavity of ***limaçon*** shape has shown the capability of highly directional light emission with a divergence angle of around 40-50 degrees, which is a big improvement to the light spreading problem.(Wiersig & Hentschel, 2008)

On the other hand, when we employ a new micro-cavity of vertically reflecting distributed Bragg reflector (DBR) structures added below and above quantum well (QW) planes, say a few active 80Å (Al) GaAs QWs, a 3D toroidal cavity is formed giving rise to helix standing waves in 3D whispering cave modes (WCMs) as shown Fig. 1 (Ahn et al., 1999). The photonic quantum ring (PQR) laser of WCMs is thus born without any intentionally fabricated ring pattern structures, which will be elaborated later. The PQR's resonant light is radiating in 3D but in a surface-normal dominant fashion, avoiding the 2D WGM's in-plane light spread problem.

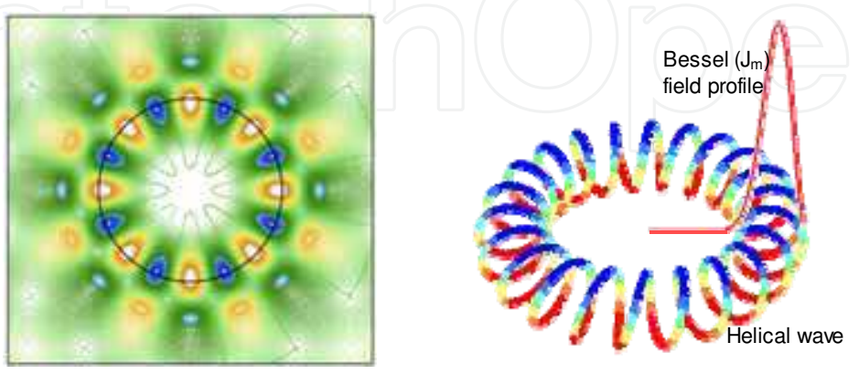

Fig. 1. Planar 2D Bessel function WGMs vs. toroidal 3D knot WCM (Park et al., 2002). The 3D WCM is a toroid with a circular helix symmetry not reducible to the simple 2D rotational symmetry

Source: Advances in Optical and Photonic Devices, Book edited by: Ki Young Kim,
ISBN 978-953-7619-76-3, pp. 352, January 2010, INTECH, Croatia, downloaded from SCIYO.COM

2. Basic properties of PQR lasers

The 3D WCM laser of PQR, whose simulation work will be shown later, behaves quite differently due to its quantum wire-like nature as follows: First of all, the PQR exhibit ultra-low threshold currents – for a mesa-type PQR device of 15 um diameter, the PQR at the peripheral Rayleigh band region lases with about one thousandth of the threshold current needed for the central vertical cavity surface emitting laser (VCSEL) of the same semiconductor mesa as illustrated in Fig. 2.

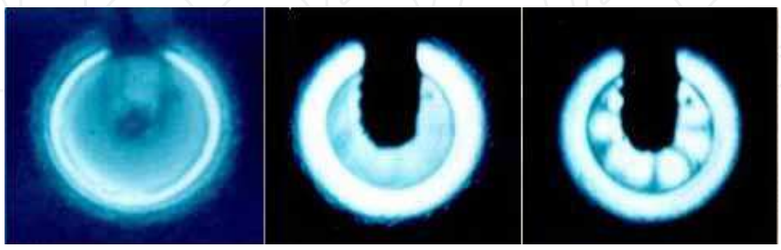

Fig. 2. CCD pictures of emisssions at 12 μA, near PQR threshold, at 11.5 mA, below VCSEL threshold, and at 12.2 mA, above VCSEL threshold, respectively.

We can however make theoretical formulae consistent with above concentric PQRs and do some calculations for comparing with the transparency and threshold current data observed. The PQR formulae can be derived by assuming that the pitch of concentric rings is 'photonic' kind of one half wavelength - optical λ/2 period: The transparency (I_{tr}: curve T) and threshold (I_{th}: curve A) current expressions for the case of PQRs occupying the annular Rayleigh region is now given by (1).

$$I_{th} = I_{tr} + I_i = N^{1D} \times W_{Rayleigh} / (\lambda / 2n_{eff}) \times \pi\phi \times (e / \eta\tau) + I_i \tag{1}$$

N^{1D} is the 1D transparency carrier density, τ the carrier lifetime, η the quantum efficiency, and I_i stands for internal loss (Ahn et al., 1999; Kwon et al., 2006). The PQR formulae are now compared with the actual data in Fig. 3, which show quite an impressive agreement except some random deviations due to device imperfections. For smaller diameters (ϕ) the active volume decreases below 0.1 μm^3, and with the cavity Q factor over 15,000. The corresponding spontaneous emission coefficient β will become appreciable enough for threshold-less lasing without a sharp turn-on threshold, which often occurs in the PQR light-current analyses. As listed in Fig. 3, the wide-spread data suggest a fuzzy ring trend growing as the device shrinks due to the growing leaky implantation boundary around the implant-isolated holes, and the hole PQR threshold data are actually approaching the curve B, whose formula is derived for the mesa by assuming that the Rayleigh region is now nothing but a piece of annular quantum well plane of random recombinant carriers instead:

$$I = N^{2D} \times W_{Rayleigh} \times \pi\theta \times (e / \eta\tau) \tag{2}$$

Figure 4 shows a collection of linewidth data being roughly inversely proportional to the device size as expected. The narrowest linewidth observed with an optical spectrum analyzer to date from a 10 um PQR is 0.55 Å at an injection current of 800 uA. We also note that with wet etching steps employed instead of dry etching, the Q factor reached up to 20,000 while the linewidth approached 0.4 Å (M. Kim et al., 2004). Although we did not

attempt it for GaAs, a CALTECH group devised a laser baking process for achieving ultrahigh Q values of multi-millions involving a SiO2 microcavity. It is interesting to be a toroidal microcavity whose 3D WCM properties is unknown yet (Armani et al., 2003; Min et al., 2004).

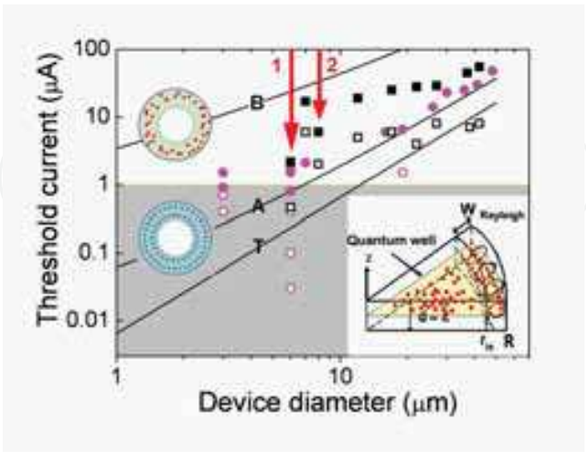

Fig. 3. Threshold curves A and B from PQR and quantum well formulae, respectively, with corresponding Rayleigh toroid schematics (defined by Rayleigh width between rin and R) and transparency curve T for the PQR case. Data for transparency (empty symbols) and threshold (solid symbols) currents: circles for PQRs and squares for PQR holes implant isolated. Data at 6 and 8 μm correspond to the case of 256×256 hole arrays without implantation (see the arrows 1 and 2).

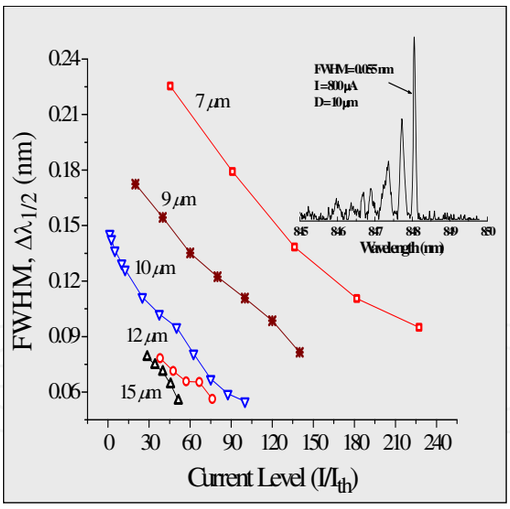

Fig. 4. Linewidth data vs. current s with various device sizes

Now we figure that the helical WCM standing wave manifold transiently induces concentric PQRs for imminently recombinant carriers present in the Rayleigh region $W_{Rayleigh}$ of the 2D quantum well. This in turn exhibits extremely small thresholds in the the μA-to-nA range with the given $\sqrt{T}$ -dependent thermal stabilities. It is attributed to a photonic (de Broglie) quantum corral effect, similar in character to the well-known electronic quantum corral image from room temperature scanning tunneling microscope studies of Au atomic island plane at a given bias.

The photonic (de Broglie) quantum corral effect imposes a λ/2 period transient ordering upon the imminently recombinant carriers, although the optical λ/2 period for GaAs semiconductor will be substantially larger than the electronic de Broglie spacing. We note that the Rayleigh region of quantum well planes is deeply buried beneath a few micron thick AlAs/GaAs Bragg reflectors not accessible for direct observation. However, recent experiments and modeling work on dynamic interactions between carriers and transient field in a quantum well plane is a close case in point (Gehrig & Hess, 2004). It thus appears that the transient quantum wire-like features considered here seem to persist within the relevant time scale through thermal fluctuations. For an ensemble of carriers randomly distributed in the regional quantum well plane of concentration 10^{12} cm^{-2} for instance, tens-of-nm scale local field-driven drifts of given carriers to a neighboring imminent PQR site should generate the proposed PQR ordering for an imminent recombination event of annihilating electron-hole pairs. For example, one can imagine a transient formation of the two separate Rayleigh rings instantly via light field-induced migration of random carriers within the $W_{Rayleigh}$ region as schematically shown for curve A in Fig. 3. We expect the standing waves in the Rayleigh region to give rise to a weak potential barrier for such a dynamic electron-hole pair process, perhaps an opposite case of extremely shallow quantum well excitons at room temperature where even the shallow barriers tend to assure at least one bound state according to square well quantum mechanics.

3. Spatio-temporal dynamic simulation of PQR standing waves and carriers

Although it is limited to 2D cases, recent spatiotemporal dynamic simulation work in a straight waveguide case (see Fig.5) faithfully reveals such a tangled but otherwise quantum-wire-like ordering of recombinant carriers undergoing some picosecond-long exciton process, consistent with the photonic quantum corral effect due to a strong carrier-photon coupling. The images of several standing light-wave-like carrier distribution patterns within a 1 micron wide quantum well stripe emerge, as a function of time from-5-to-8 psec after about 5 psec chaotic regime as indicated along the horizontal time axis of 10 psec full range, shown in Fig. 6 (Kwon et al., 2009). They are curiously reminiscent of the tangled web of the 2D electron gas due to impurity atom potentials studied by a Harvard group (Topinka et al., 2003).
The assumed concentric quantum ring pattern of carrier distribution within the Rayleigh region is not observable directly since they are buried below a few micron thick top DBR structures. Instead the CCD pictures are their distant images refracted and smeared out through the semiconductor medium.
As said before, the resonance of the PQR laser results in 3D WCM of helical standing waves, which is surface-normal dominant, in contrast to the in-plane 2D WG mode. The data taken with a home-built solid angle scanner setup, which will be discribed later, shows a tangential polarization dominance which supports strong carrier-photon couplings behaviors needed for the PQR formation (Kim et al., 2007)

4. 3D WCM mode analysis and single mode PQR laser

A 3D WCM mode analysis, based upon the helix mode of the PQR consisting of a bouncing wave between the two DBRs and a circulating wave of in-plane total reflection, gives an angular quantization rule for easy PQR mode analysis of 3D spectra taken with tapered single mode fiber probes as shown in Fig. 7 (Bae et al., 2003).

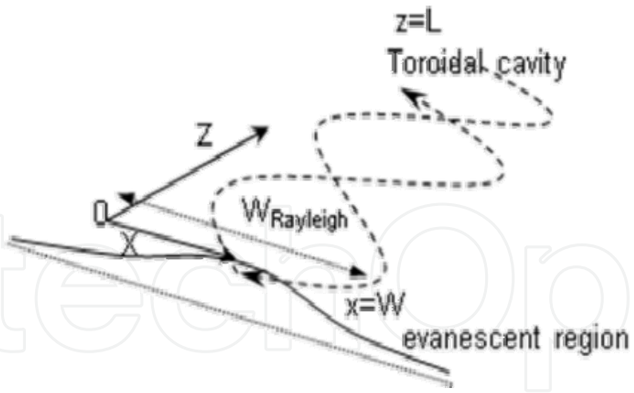

Fig. 5. Flattened top view of helix modes within a Rayleigh bandwidth

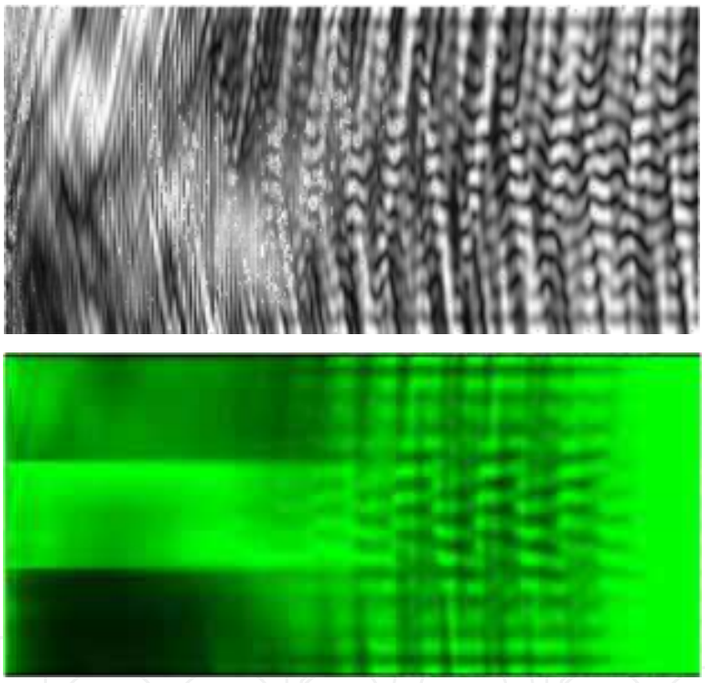

Fig. 6. Spatiotemporal 2D simulation results: top –standing waves are formed after a few picoseconds of chaotic regime in the case of flattened and straight rectangular wave guide version [x-axis span of 10 psec.]; bottom – carrier distribution dynamics shown for 10 picoseconds, where similar patterns emerge after a few psec. Y-axis indicates a 1 um wide central waveguide in the middle of 3 um boundary.

For single mode lasers we have made non-conventional PQRs of hyperboloid drum shape like Figs. 8 (a) and (b) (Kim et al., 2003) having a submicron active diameter with $\phi = 0.9\ \mu m$, where as its top region of a few micron diameter serves as metallic contact area for electro pumping. Figs. 8 (c) and (d) show the threshold data with a 0.46 $\AA$ linewidth exhibit the smallest threshold of about 300 nA, (Yoon et al., 2007) observed so far among the injection lasers of quantum well, wire, or dot type to the best of our, although the external quantum efficiency observed right after the threshold is poor suffering from the soft lasing turn-on behavior here.

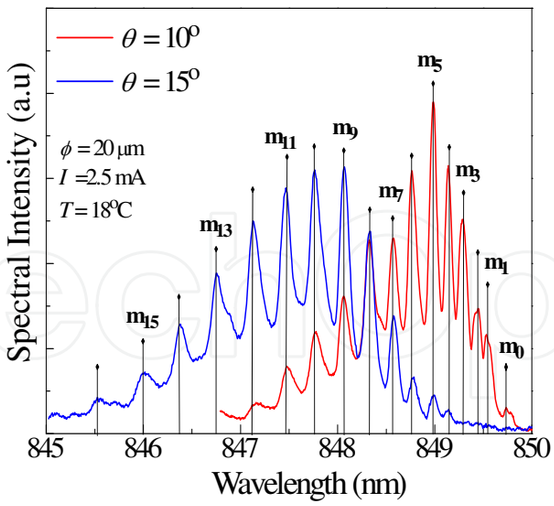

Fig. 7. Angular measurement set up for 3D WCM and some typical spectra

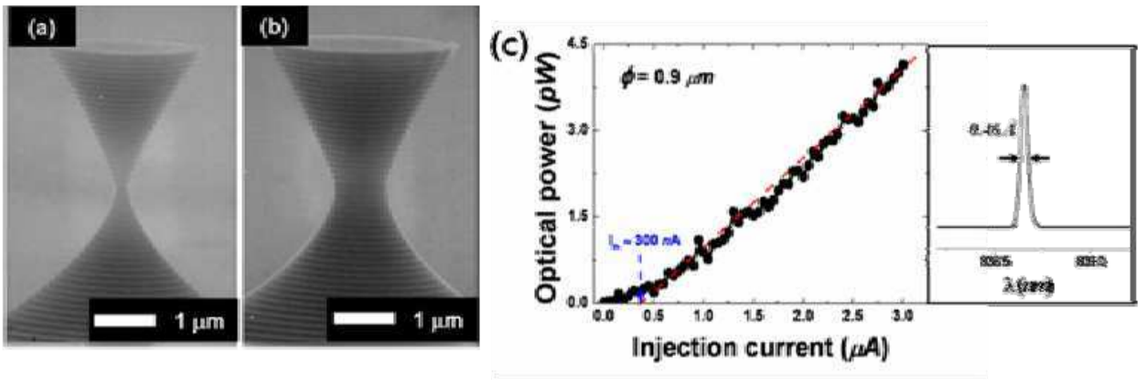

Fig. 8. Hyperboloid drum PQR: SEM micrograph, L-I curve, and single mode spectrum

5. Mega-pixel laser chips of photonics quantum ring holes

We have succeeded in fabricating the high density array chip of PQR hole lasers of one mega (M) integration. 1M PQR hole array chips has ultra low threshold current of 0.736 nA per single hole due to photonic crystal-like cooperative effect (Kwon et al., 2008) 1M PQR hole laser array chip is fabricated in tandem type with four 256K PQR hole arrays for uniformly injecting current on the device surface. The used epitaxial wafer structure of a p-*i*(MQW: multi quantum well)-n diode was grown on an n-type GaAs (001) substrate by metal-organic vapor-phase epitaxy. The structure consists of two distributed Bragg reflector (DBR) mirrors surrounding the *i*-region of a one-λ cavity active region (269.4 *nm* thick) including three GaAs/$Al_{0.3}Ga_{0.7}As$ quantum well structures, tuned to yield a resonance wavelength of 850 *nm*. The p- and n- type DBR mirrors consist of alternating 419.8 *Å* $Al_{0.15}Ga_{0.85}As$ and 488.2 *Å* $Al_{0.95}Ga_{0.05}As$ layers, 21.5 periods and 38 periods respectively. Figures 9(a) and (b) show scanning electron microscopy (SEM) images for top view and cross section of 1*M* PQR hole laser array, respectively, whose SEM pictures exhibit a bit rough cross section as compared with single device side walls in Figs. 9(c) and (d).

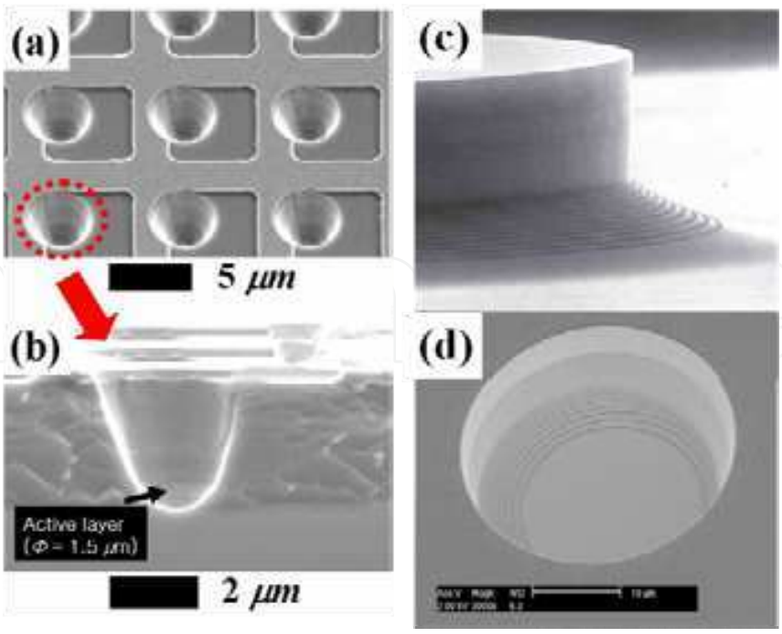

Fig. 9. (a) Top and (b) cross section SEM images of 1M PQR hole array (c) SEM micrographs of mesa and hole type PQR structures.

Figure 10(a) shows the CCD images of the illuminant 1M PQR hole array near the transparent current, 0.08 *A* (80 *nA/cell*) and near the threshold current, 0.7 *A* (700 *nA/cell*). To measure the *L-I* curve for 1M PQR hole array, we used a conventional power meter (Adventest Mo.Q211) and measured directly 1M PQR hole array. For measurement of threshold current and angle-resolved spectra shown in Fig. 11, we used a piece of 1/32M PQR hole array, because the total size of 1M PQR hole array chip is 1 cm^2 which is larger than the aperture size (diameter = 0.8 *cm*) of the power meter.

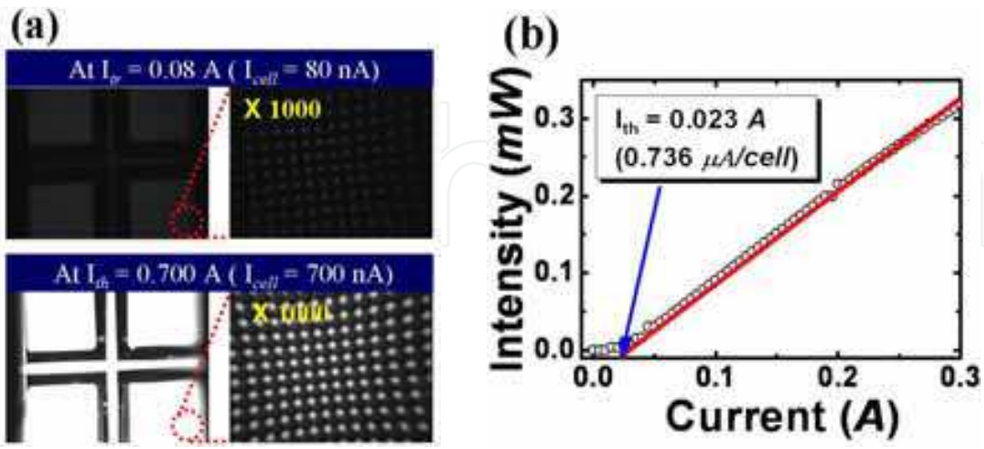

Fig. 10. (a) CCD (right) and 1000 times magnified (left) images of the illuminant 1M PQR hole array (4x250K arrays) at transparent and near threshold current. (b) *L-I* curve of 1/32M PQR hole array chip. As shown in Fig. 2(b), the threshold current is measured 0.736 *μA/hole* by using linear fitting.

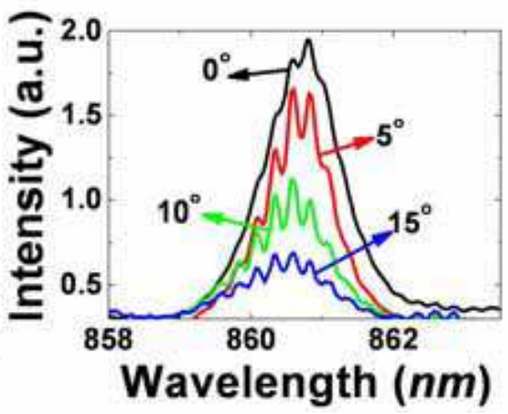

Fig. 11. (color online) Angle-resolved spectra of single hole among 1M PQR hole array at 32 *μA/hole*.

6. PQR light sources for display

We now discuss the properties of the PQR technology applicable for the next generation display. Light-emitting diodes (LEDs) display has become a multi-million dollar industry, and it is growing. LEDs are under intensive development worldwide for advanced display applications (Schubert, 2003)

However, high- power LEDs being bulk devices faces problems like the notorious LED extraction factor associated with internal heating problems, large concentration of impurity scatters, and low modulation frequencies less than MHz ranges. Although the LED performances are improving, lasers can be the alternative answer with the usual GHz range modulation capability. In particular, the PQR laser is an attractive candidate for next generation display, based upon the special PQR characteristics as explained in the preceding sections like extremely low threshold currents, thermally stable spectra, and high-density chip capabilities. The PQR of WCMs can have both concave and convex modes, which are the fundamental properties exploited for fabricating high power flower type PQR lasers as elaborated in the end for display applications.

The high power PQR laser properties will now be presented to compare with conventional LEDs, in terms of properties such as power-saving features, color purity, luminous efficiency, and beam shape properties:

The spectral data for a conventional LED has a linewidth of about 25 nm which may be reduced further down to several nm in the case of resonant cavity LEDs, while the linewidth of the PQR is usually around or below 0.1 nm, as illustrated in Fig. 12, the spectra for a PQR of ϕ = 7 μm. Namely, if the linewidths of the PQR and LED are about 0.1 and 25 nm, respectively, the electric power consumption of the PQR is about 1/250 of the LED power consumption. It means that the low threshold current and sharp discrete mode PQRs offer high brightness as LED with much less amount of electric current because the sum of each sharp peak can replace the broad peak of LED spectrum. The PQR's color purity is about 1 which means high color rendering ability.

Fig. 13(a) shows the emission image of the 16x16 mesa type red PQR laser array. A single red PQR emission reveals two different regions at a given injection current (I=24uA/cell). The PQR lasing occurs in the periphery of the active disk called the Rayleigh band and the

LED emission occurs in the middle part of the disk. Luminous efficiency of the 16x16 red PQR array is 7.20lm/w at the 670nm wavelength, which, if translated to 620nm with the color conversion factor multiplied, becomes two times better than the commercial 620nm LED products as shown in Fig. 13(b).

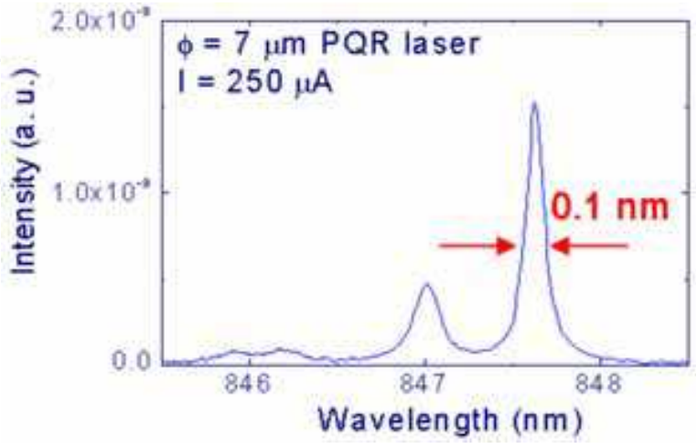

Fig. 12. Spectrum of ϕ = 7 μm PQR laser.

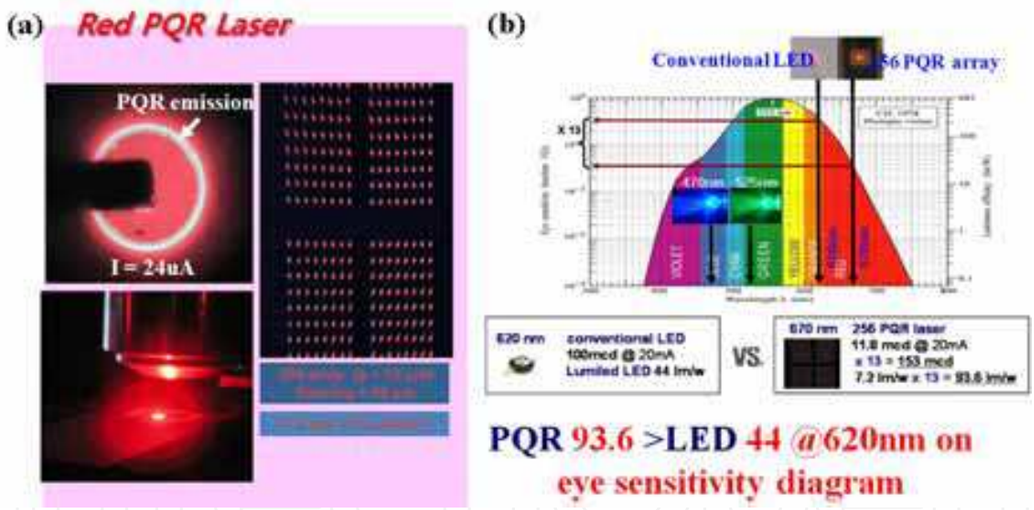

Fig. 13. Photometric characteristics (PQR vs LED) (a) Emission image of the 16x16 red PQR laser array (Φ= 7um, pitch = 68um). (b) Comparison of the photometric characteristics between 16x16 red PQR array and conventional high power LED.

Blue GaN surface-emitting lasers are notoriously difficult to fabricate and we give a couple of recent examples of GaN surface-emitting laser work: First, a photonic crystal based surface emitting laser was developed Japanese researchers where their photonic crystal structure consists of a 2 dimensional array of airholes. Their result is however far from practical applications. The threshold current obtained was rather large as 6.9A in pulsed mode operation (Yoshimoto et al., 2008)

A Taiwanese group also reported GaN hybrid VCSEL laser work where they used n type crack- free AlN/GaN DBR and Ta_2O_5/SiO_2 dielectric DBR. Still, the operation was at liquid

nitrogen temperature (77K) (Lu et al., 2008). Practical GaN VCSEL lasers thus seem very hard to achieve CW at room temperature.
On the other hand, we are making the blue PQR lasers which is CW operated at room temperature lasing in 3D but emitting dominantly in surface normal direction. Our blue PQR lasers with wavelengths between 420 and 470nm are fabricated using a GaN wafer with sapphire substrates removed via laser lift-off (LLO) procedures (Fig. 14).
The multi mode lasing spectra from the blue PQR as shown in Fig. 15 and this tentative result was reported in the reference (Kim et al., 2006).

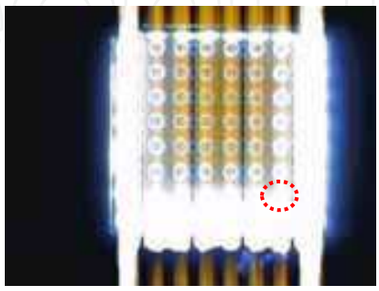

Fig. 14. Blue PQR array with the edge region affected by spontaneous background emission (in red circle).

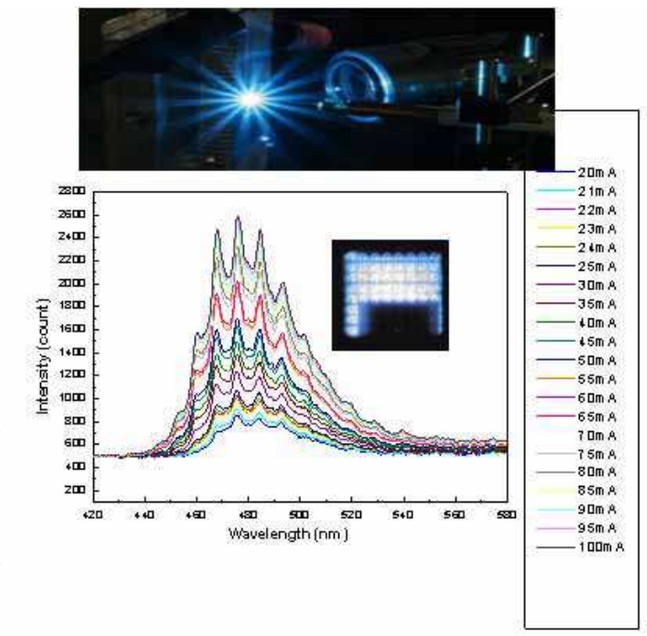

Fig. 15. Multimode spectra from a blue PQR (in red circle in Fig. 14) CW at room temperature with I = 60uA/cell to 1.63mA/cell.

7. PQR laser beam propagation characteristics

For 3D beam profile studies, we have used a home-built 2D/3D single photon scanning system for measuring the PQR beam profile and polarization with a resolution of 0.5μm/step.

As shown in the schematic Fig. 16, a tapered single mode fiber tip about 300nm in diameter was made by chemical etching for the photon collection, and a step motor generates relative motions of the tip against probed PQR laser device. The collected photon signal goes through single photon counting module, photon counter, and computer.

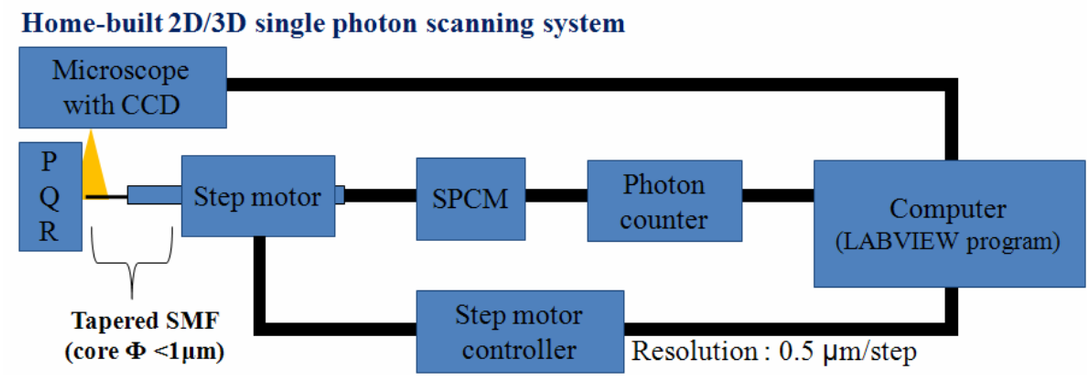

Fig. 16. A schematic diagram of home-built 2D/3D single photon scanning system.

Figure 17 shows some 2D scan results over a scan area of 60x60 um square, where, on the surface of the PQR, Fig. 17(a) exhibits that the emission pattern of the PQR beam is Laguerre Gaussian for the case of a mesa PQR, and Fig. 17(b) shows another Laguerre Gaussian pattern for the case of hole PQRs.

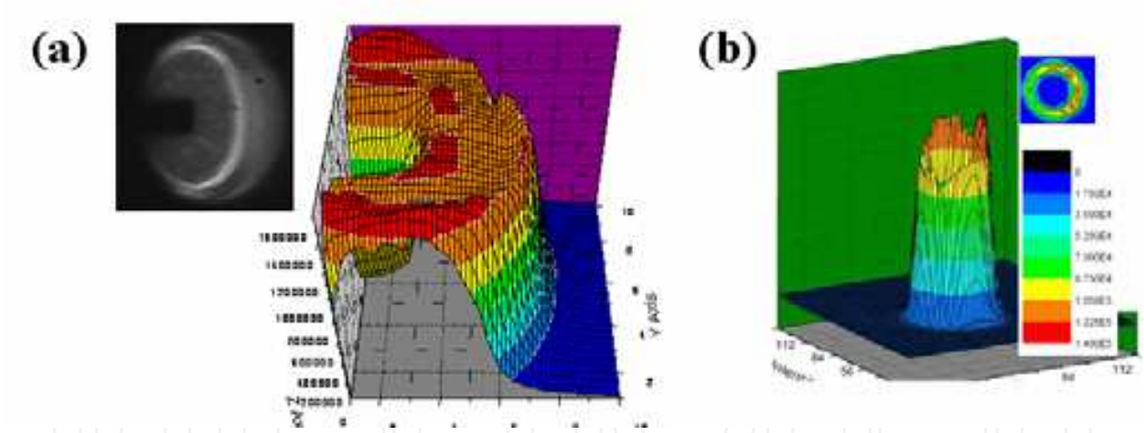

Fig. 17. (a) Lagurre Gaussian beam of the mesa PQR (b) Lagurre Gaussian beam of the hole PQR

8. Fabrication of micro collimators for PQR beam guiding

Laser printers with mechanically rotating polygon mirrors have been used widely in offices, whereas new LED printers, quiet and all-electronic drive circuitry with no moving parts, begin to replace them. However, the LED, being a spontaneous emission device with some disadvantages as stated earlier, can further be replaced by an efficient laser like the PQR laser diode with extremely low threshold currents and $\sqrt{T}$ -dependent thermally stable spectral properties which are good for fast, high density array applications. Moreover, typical LED printers use selfoc-lens arrays (SLAs) to concentrate and guide individual light,

but the expensive SLA technology is complicated. We note that the PQR laser with the micro collimator (MC) for non-parallel to parallel beam guiding described previously may replace the LED + SLA technology. In order to find such a possibility, we will now describe several fundamental features of the PQR laser such as the beam shape and propagation behaviors, MC-guided PQR beams, beam divergence, and high power capabilities.

For beam divergence studies, Fig. 18(a) represents a PQR emission pattern observed from a device of a 48um diameter which is rather close to the Lambertian emission pattern of a conventional LED. However noting that the Gaussian beam is characterized by the spot size and divergence angle θ, recent 3D PQR beam profile studies of 15um PQR lasers also show possibilities of controlling the beam divergence to the narrower ranges, for example a divergence angle of θ = 2 x 6.3 degree as shown in Fig. 18(b). This analysis results from the 3D scans made at 30, 60 and 90 um heights respectively as shown in Figs. 18(c),(d) and (e), where divergence points are determined as half maximum intensity points. We find from the 3D scans that the initial beam profile of Laguerre Gaussian is evolving to Gaussian as a function of scan height. The beam shapes are nearly Gaussian at 30um height and perfectly Gaussian at 60um height, which gives rise to a cross-over from Laguerre Gaussian to Gaussian at around 40~50um height. In our divergence analysis we may regard the PQR ring as a Bessel beam formed at the rim of the PQR device surface from an imaginative point light at the origin located deep below the device surface.

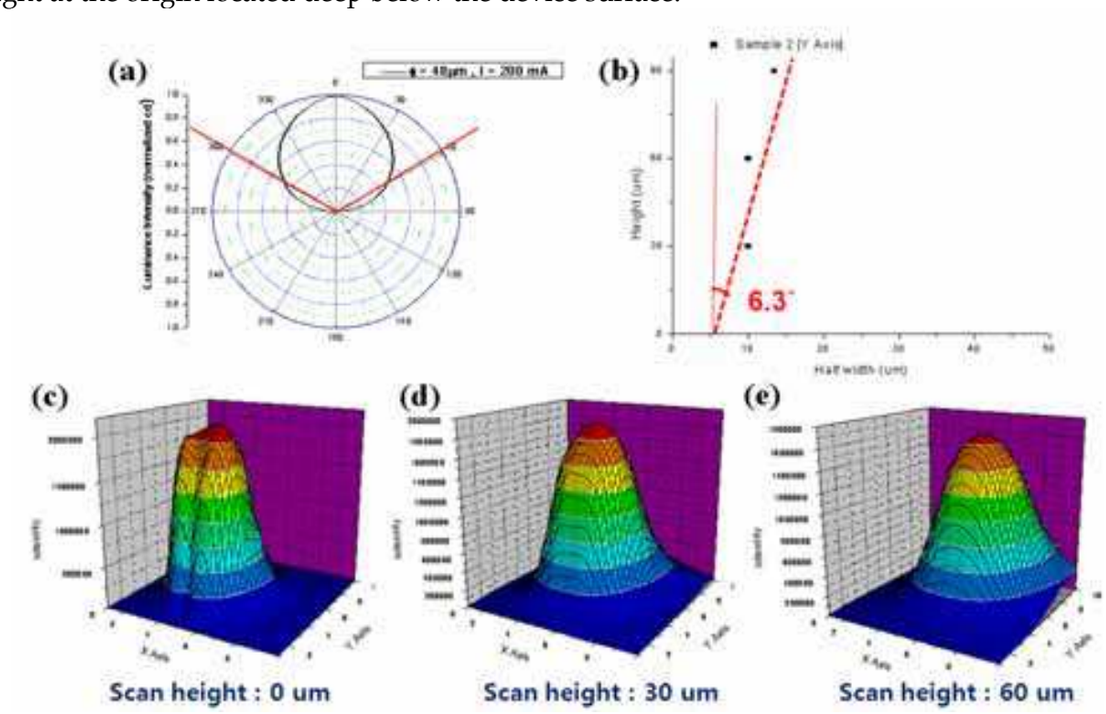

Fig. 18. (a) Lambertian profile of a PQR (b) Divergence angle of a PQR (c) (d) and (e) represent beam scans taken at different heights, 0, 30, and 60 um

For practical system applications of light sources one often has to find how to control, or focus and guide, the laser beam. Therefore we now turn to an active beam control method employing convex and concave MCs for focusing and guiding the PQR light through lens media and free space. The convex and concave lenses of the MC are designed and fabricated as shown in Figs. 19(a) and (b).

A master lens array is made by a photoresist (PR) reflow method, and the PR microlens array is transferred to a polydimethyl-siloxane (PDMS) master by a casting method. Finally, the PDMS is spin-coated again on the PDMS master, whose details are described (O'Neill & Sheridan, 2002). Fig.19(a) are SEM images of the final micro lens arrays fabricated to be 17um in diameter and 10um in height for the convex lenses (top) and 36um in diameter for the concave lenses (bottom).

Fig. 19(c) represents a series of CCD snap shots taken at various distances from the PQR laser surface where the microlens set on the fifth spot happens to be absent. The snap shots vividly shows that the propagating Gaussian beam is guided to the point of minimum spot at 160um distance and reconstructs the original PQR laser image at around 400um distance. The fact that the missing 5th spot is not affected by any possible neighbor's diffraction ghost means that the PQR beam behaves as a Bessel beam.

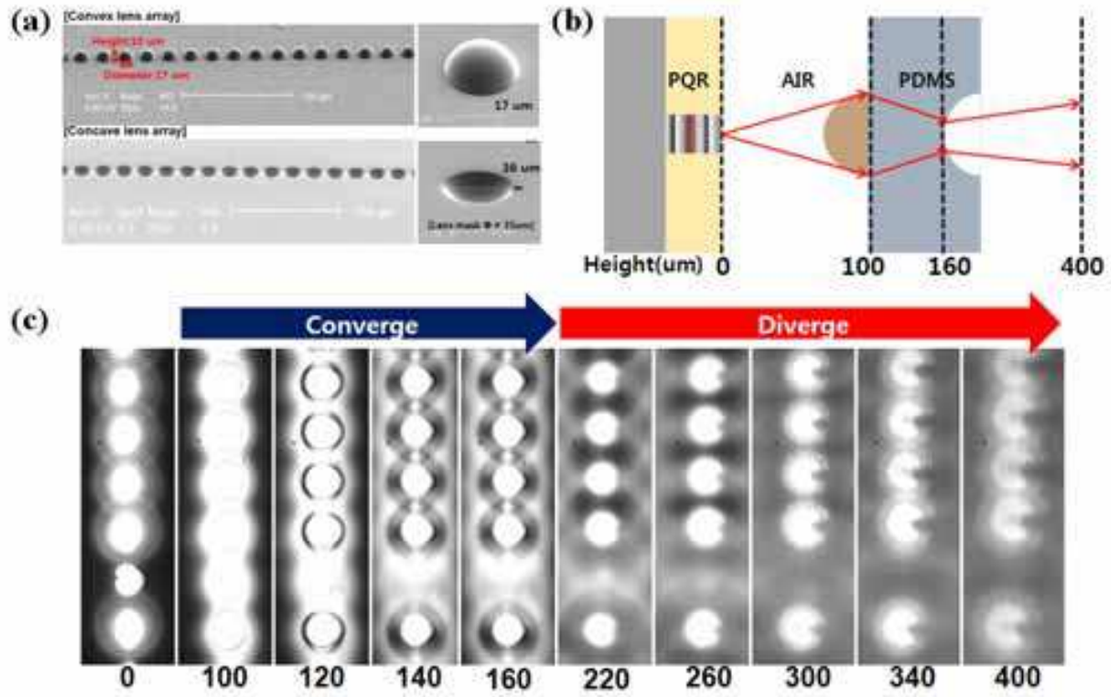

Fig. 19. (a) Convex and concave lens arrays. (b) Outline of beam guiding optics. (c) CCD snap shots taken at different distances.

9. Design and SEM images of flower PQR laser

We now describe the design and fabrication of the new flower PQR laser for output power enhanced about 5 times the power expected from regular circular PQR lasers of the same size, where 4, 8, and 12 –petal flower designs, combining concave and convex whispering cave modes, result in the increased overall quantum wire length of the emitting PQR within the same device area.

As shown earlier in Fig. 13(a), the PQR region emitted first and much brighter than the central LED emission region, which means a very high emission efficiency of the PQR laser. We however note that the emission region is occupied mostly by the central LED emission

in this case. That is the reason why we make use of the flower design in enhancing the PQR light output power since the increase of the PQR region by sacrificing the central LED area are achieved with more number of petals in a fixed diameter mesa. When the current density is the same, the more the number of petals, say the more the area of peripheral PQR region, the more the flower PQR laser intensity. We however note that the total length of peripheral PQR curves is to be smaller than the critical length for GaAs PQRs, corresponding to the device perimeter of a critical diameter (ϕ= ~50 μm), so that the quantum ring whispering cave mode begins to disappear (Kwon et al., 2006).

The photonic quantum ring (PQR) laser is an attractive candidate for high-density "laser" displays, given the unique operating characteristics attendant on its quantum-wire-like nature, such as extremely low threshold currents and thermally stable spectra in the typical operating-temperature range. When vertical mesa cavities are made of λ/4 Al0.92Ga0.08As/Al0.16Ga0.84As distributed Bragg reflector (DBR) structures added below and above an active region of multi-quantum wells (QWs) of 7nm thick GaAs each separated by 8nm thick barriers of Al0.3Ga0.7As, emitting at 850nm. Moreover, we have observed unusual convex WCMs from reverse-mesa (=hole)-type micro-resonators, whose WCMs we interpreted with respect to gain-guiding and photonic quantum corral effects. We now re-stress that the light output power observed enhances roughly in proportion to the number of petals of the flower PQR laser, up to the point where the total PQR perimeter reached a critical length corresponding to that of a circular PQR laser of about 50 μm diameter.

Circular and 4, 8, and 12-petal flower PQR lasers of the same overall diameter (Φ = 20 μm) for example are designed and fabricated. We can calculate the various multi-petal PQR perimeters' total lengths corresponding to the respective quantum wire lengths of Rayleigh band. The circular PQR of Φ = 20 μm has a peripheral PQR length of about 63 μm. When the number of petals, in the same overall diameter (Φ = 20 μm) of flower, is 8, the total peripheral PQR length is about 84 μm, and when the number is 12 then the total length is about 115 μm. The increased number of petals is more or less proportional to the growth of flower PQR output power, which is roughly proportional to the total peripheral PQR length. The SEM image of a 12-petal flower PQR laser is shown as an example in Fig. 20. Mesas 4.2

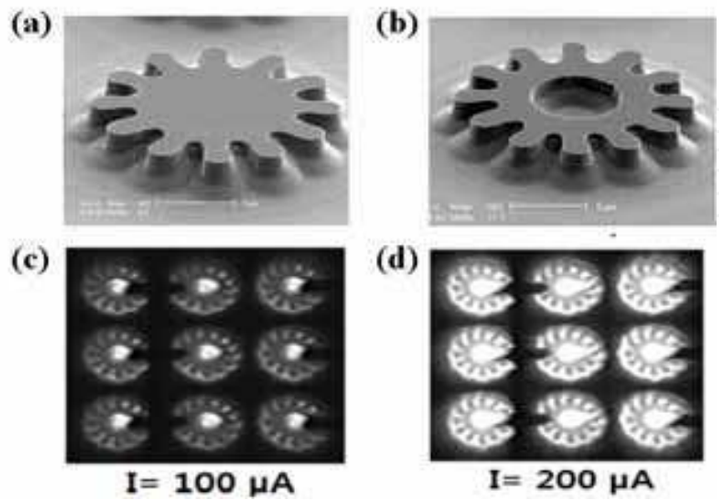

Fig. 20. SEM images of 12-petal flower PQRs (a) without hole (b) with hole (c) and (d) show illuminant PQRs at different injection levels.

μm high were etched by chemically assisted ion beam etching (CAIBE) with a photoresist mask. The smoothness of the side wall is an important factor in minimizing the spectral linewidth of PQR lasers. For side wall smoothness and highly anisotropic etching, we tilt and rotate the substrate in the CAIBE chamber during the etching process while adding BCl3 gas to facilitate Al2O3 removal in addition to an Ar/Cl2 gas mixture. Full details are given in a reference (Kim et al., 2004)

10. Fabrication of high power flower PQR laser

Fig. 21 shows emission images of various flower PQR lasers of Φ = 20 μm. For comparison, we simultaneously fabricated a circular mesa PQR laser of Φ = 18 μm. A tremendous intensity build-up occurred after increasing injection currents, so that appropriate neutral density filters had to be used for intensity attenuation. PQR lasing occurs along the perimeter of the active disk called the Rayleigh bandwidth, 0.63 μm width for Φ = 20 μm (Ahn et al., 1999), while LED emission occurs in the central bulk region of the PQR mesa. A threshold of 28 μm (= 11 A/cm2), observed through ring pattern schemes as shown in Fig. 21, is apparently smaller than the threshold range around 20 – 30 A/cm2 as estimated via usual extrapolation schemes, where the convex TIR effect of 'hole' PQR portions is involved in addition to the 'soft lasing turn-on' behavior (Kim et al., 2009).

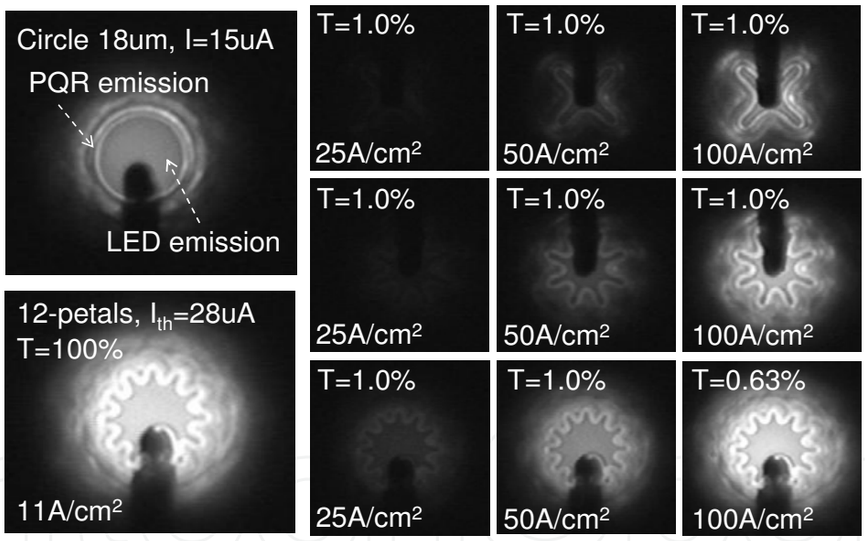

Fig. 21. Various emission patterns of 4-, 8-, 12- petal flower PQRs

As mentioned earlier, the flower design enhances the PQR light output power, thanks to the increase of the effective PQR region, while reducing the central LED area by means of a greater number of petals in a given diameter mesa. When the current density is the same, the greater the number of petals (the larger the area of the peripheral PQR region), the higher the flower PQR laser intensity. We can describe the light intensity as a function of the number of petals. For the devices with 20um width, the optical output power increased when the number of petals increased (Fig. 22). As the number of petals increased, the length of peripheral PQR region is larger so that the region occupied by the PQR emission in the whole emission region increased, leading to the final increase of the optical output power.

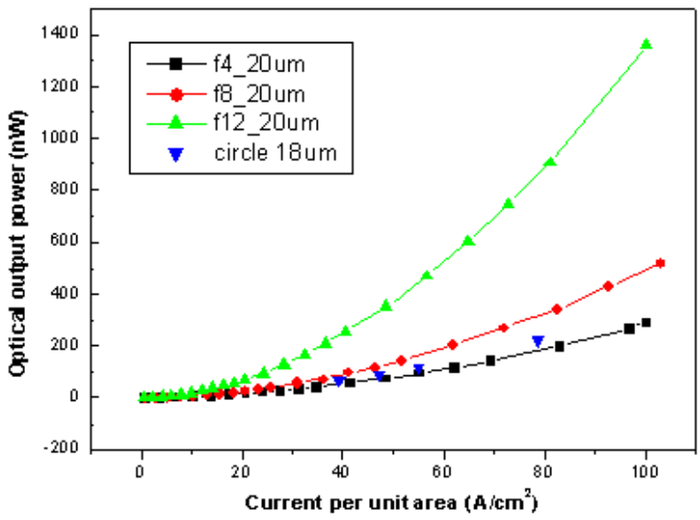

Fig. 22. Optical output power comparison (ϕ= 20 μm)

11. Panel-less TV display scheme with RGB PQR lasers

Today the market of display is dominated by LCD and PDP flat panel display (FPD) TVs, while expensive wider panels become too heavy to handle. The PQR laser is an attractive candidate for next generation display. We are currently developing a panel-less laser image chip for TV display using addressable PQR (photonic quantum ring) laser-pixels. For high brightness, wide-picture and full-color high definition TVs, we can design optimized projection systems involving RGB PQR laser array strategies, and lens optics for image magnification and projection similar to a light engine, where the RGB PQR display module will be the basic building block filling up the 2D/3D lattice of infinitely expansible TV display. Fig. 23 is a schematic diagram of a beam combination demonstrator for RGB color display.

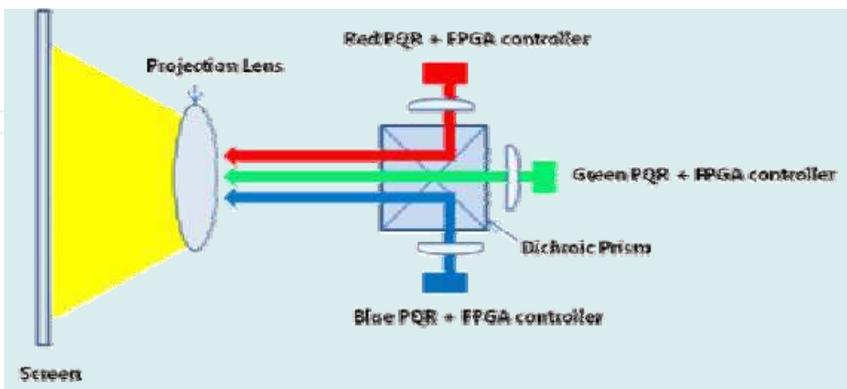

Fig. 23. A beam combination example

In the case of red beam, for example, the schematic may involve 1 or 2 lenses for beam guiding, resulting in an instantaneous frame of red beam scan implemented through an arrangement of optical components as shown Fig. 24. The blue and green beam combination structures are under development.

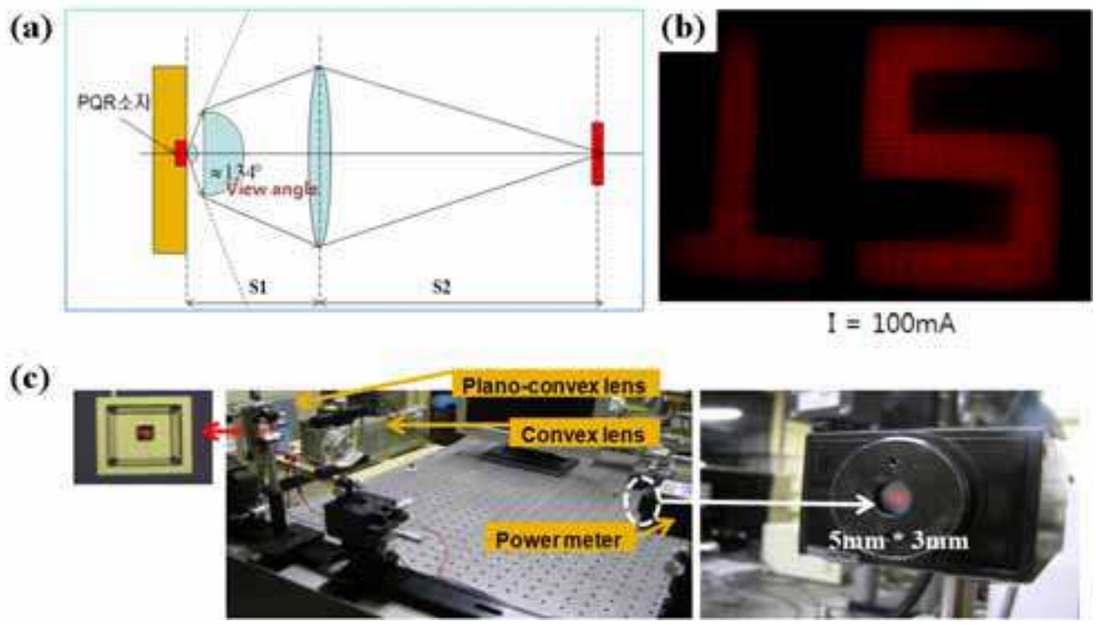

Fig. 24. (a) Red beam optics outlined. (b) Red letter image (c) Experimental set up of the optical components

12. Conclusions

We have presented studies of 3D WCM of PQRs. The 3D WCM laser is surface-normal dominant and has no in-plane resonance while the 2D WGM laser is in-plane dominant. Also the 3D WCM's major polarization state favors such a strong carrier-photon coupling that the powerful transient coupling generates PQRs, i.e., a photonic quantum corral effect. This gives rise to the low threshold currents and thermally stable spectra, important for easy optical mega-pixel ('Omega') chip fabrications which will be useful for next generation TV display. We have also presented Gaussian beam properties and guiding work of the PQR laser.

13. References

Ahn, J. C. et al., Photonic quantum ring, *Phys. Rev. Lett.* 82, No.3 pp 536-539 (1999).

Armani, D. K. et al., Optical microcavities, *Nature* 421, 925 (2003); Min, B. et al., Erbium-implanted high-Q silica toroidal microcavity laser on a silicon chip, *Phys. Rev*. A70, 033803 (2004).

Bae, J. et al., Spectrum of three-dimensional photonic quantum-ring microdisk cavities: comparison between theory and experiment, *Opt. Lett.* 26, 632 (2003).

Feidhlim, T. & O'Neill, J., Photoresist reflow method of microlens production Part I, *International Journal for Light and Electron Optics*, 113. 391 (2002)

Gehrig ,E. et al., Dynamic filamentation and beam quality of quantum-dot lasers, *Appl. Phys. Lett.* 84, 1650 (2004).

Ide, K. et al., LaGuerre–Gaussian Emission Properties of Photonic Quantum Ring Hole-Type Lasers, *IEEE Trans. Nano.* 7, 185 (2008).

Kim, D. & Kwon, O., Polarization characteristics of photonic quantum ring laser with three-dimensional whispering gallery resonances, *J. Appl. Phys.* 102, 053104(2007).

Kim, J. Y. et al., Fabrication of Photonic Quantum Ring Laser using Chemically Assisted Ion Beam Etching, *J. Vac. Sci. Technol*. B. 19, 1334 (2001).

Kim, J. Y. et al., Effect of surface treatment on leakage current of GaAs/AlGaAs laser microcavitys, *Appl. Phys. Lett.* 82, 4504 (2003).

Kim, M. et al., Wet etching fabrication of photonic quantum ring laser, *J. Appl. Phys.* 96, 4742 (2004).

Kim, Y. C. et al., PQR laser can outdo LED, *IEEE-NMDC 2006* 21-24 (2006), Gyeongju, Korea; Laser Focus World (March 2008).

Kwon, O. et al., Photonic quantum ring laser of 3D whispering cave mode, *Microelectronics Journal,* 40, 570 (2009)

Kwon, O. et al., Hole emitter of photonic quantum ring, *Appl. Phys. Lett*, Vol. 89, 11108 (2006)

McCall, S. L. et al., Whispering-gallery mode microdisk lasers, *Appl. Phys. Lett.*60, 289 (1992).

Noeckel, J. & Stone D., Ray and wave chaos in asymmetric resonant optical cavities, *Nature* 385, 45-47 (1997); Gmachl, C., High-power directional emission from microlasers with chaotic resonators, *Science* 280, 1556 (1998).

Park, B. H. et al., Chiral wave propagation manifold of the photonic quantum ring laser, *Appl. Phys. Lett.* 81, 580 (2002).

Topinka, M.A. et al., Imaging Coherent Electron Flow, *Physics Today* 56, 12 (2003).

Wiersig, J. & Hentschel, M., Combining Directional Light Output and Ultralow Loss in Deformed Microdisks, *Phys. Rev. Lett.* 100, 033901 (2008)

Yoon, J. H. et al., Single mode photonic quantum ring laser fabricated in hyperboloid drum shape, *J. Appl. Phys.* 103, 053103 (2008)

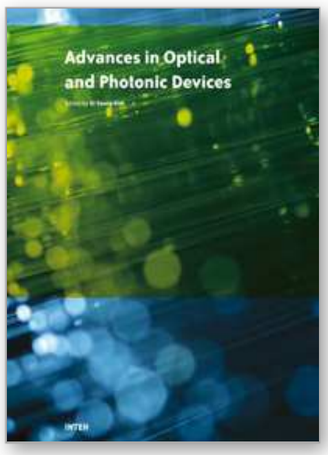

Advances in Optical and Photonic Devices

Edited by Ki Young Kim

ISBN 978-953-7619-76-3
Hard cover, 352 pages
Publisher InTech
Published online 01, January, 2010
Published in print edition January, 2010

The title of this book, Advances in Optical and Photonic Devices, encompasses a broad range of theory and applications which are of interest for diverse classes of optical and photonic devices. Unquestionably, recent successful achievements in modern optical communications and multifunctional systems have been accomplished based on composing “building blocks” of a variety of optical and photonic devices. Thus, the grasp of current trends and needs in device technology would be useful for further development of such a range of relative applications. The book is going to be a collection of contemporary researches and developments of various devices and structures in the area of optics and photonics. It is composed of 17 excellent chapters covering fundamental theory, physical operation mechanisms, fabrication and measurement techniques, and application examples. Besides, it contains comprehensive reviews of recent trends and advancements in the field. First six chapters are especially focused on diverse aspects of recent developments of lasers and related technologies, while the later chapters deal with various optical and photonic devices including waveguides, filters, oscillators, isolators, photodiodes, photomultipliers, microcavities, and so on. Although the book is a collected edition of specific technological issues, I strongly believe that the readers can obtain generous and overall ideas and knowledge of the state-of-the-art technologies in optical and photonic devices. Lastly, special words of thanks should go to all the scientists and engineers who have devoted a great deal of time to writing excellent chapters in this book.

How to reference

In order to correctly reference this scholarly work, feel free to copy and paste the following:

O’Dae Kwon, M. H. Sheen and Y. C. Kim (2010). Photonic Quantum Ring Laser of Whispering Cave Mode, Advances in Optical and Photonic Devices, Ki Young Kim (Ed.), ISBN: 978-953-7619-76-3, InTech, Available from: http://www.intechopen.com/books/advances-in-optical-and-photonic-devices/photonic-quantum-ring-laser-of-whispering-cave-mode

INTECH
open science | open minds

InTech Europe
University Campus STeP Ri
Slavka Krautzeka 83/A
51000 Rijeka, Croatia
Phone: +385 (51) 770 447

InTech China
Unit 405, Office Block, Hotel Equatorial Shanghai
No.65, Yan An Road (West), Shanghai, 200040, China
中国上海市延安西路65号上海国际贵都大饭店办公楼405单元
Phone: +86-21-62489820

Fax: +385 (51) 686 166
www.intechopen.com

Fax: +86-21-62489821

IntechOpen